modelling

MDPI

Article

Finite Element Modeling and Analysis of RC Shear Walls with Cutting-Out Openings

Islam M. Saad [1], Heba A. Mohamed [2], Mohamed Emara [2], Ayman El-Zohairy [3,*] and Sherif El-Beshlawy [1]

[1] High Institute of Engineering at 6 October, Culture and Science City, Giza 12592, Egypt; eslam-eng@csi.edu.eg (I.M.S.); beshlawys@csi.edu.eg (S.E.-B.)
[2] Structural Engineering Department, Faculty of Engineering, Zagazig University, Zagazig 44519, Egypt; hebawahbe@zu.edu.eg (H.A.M.); mremara@eng.zu.edu.eg (M.E.)
[3] Department of Engineering and Technology, Texas A&M University-Commerce, Commerce, TX 75429, USA
* Correspondence: ayman.elzohairy@tamuc.edu; Tel.: +1-903-468-8683

Abstract: In recent decades, reinforced concrete (RC) shear walls have been one of the best structural solutions to resist lateral load in high-rise buildings. Shear wall openings are essential for preparations and architectural requirements, which weaken the wall, reducing bearing capacity, energy absorption, and stiffness while also causing stress concentrations. This paper presents a comprehensive finite element (FE) investigation of the behavior and performance of RC shear walls with openings and subjected to lateral loads. The study aims to evaluate the influence of various parameters, such as opening location, size, wall aspect ratio, axial load, and concrete strength, which affect the performance of shear walls. FE models were developed to simulate the seismic response of RC shear walls under the combined effect of constant axial and lateral loads. The obtained results from the FE model showed a successful validation using the experimental data available in the literature. The FE analysis results demonstrate that the inclusion of lower openings leads to a 25% decrease in the bearing capacity of the wall when compared to the upper openings. Moreover, it was observed that augmenting the sizes of the openings and the aspect ratios of the wall resulted in declines in the strength, stiffness, and energy absorption capacity of the wall while simultaneously enhancing the ductility and displacement of the RC shear walls.

Keywords: RC shear walls; openings; finite element modeling; aspect ratio; compressive strength

Citation: Saad, I.M.; Mohamed, H.A.; Emara, M.; El-Zohairy, A.; El-Beshlawy, S. Finite Element Modeling and Analysis of RC Shear Walls with Cutting-Out Openings. *Modelling* **2024**, *5*, 1314–1338. https://doi.org/10.3390/modelling5030068

Academic Editor: José António Correia

Received: 19 July 2024
Revised: 8 September 2024
Accepted: 11 September 2024
Published: 19 September 2024

1. Introduction

Reinforced concrete shear walls have become a crucial structural system for providing buildings or structures with the necessary lateral strength to withstand lateral loads, especially earthquake loads. These walls can be constructed as monolithic or precast reinforced shear walls. Precast shear walls are advantageous for projects requiring speed, precision, and repetitive construction, while monolithic shear walls are better suited for customized designs and superior seismic performance due to their continuous nature. To address the modern challenges posed by architectural modifications, such as the creation of random openings in shear walls, it is crucial to thoroughly examine and assess the behavior of reinforced concrete shear walls in resisting both horizontal and vertical loads. These modifications are often introduced to accommodate architectural, mechanical, and installation requirements, necessitating a deeper understanding of their impact on the structural integrity of buildings. Whenever possible, openings are avoided in RC structural parts. Openings in RC shear walls significantly impact their structural capacity by reducing load-bearing capacity, increasing stress concentration, altering load distribution, and increasing deformation and drift. Avoiding openings in RC shear walls helps maintain structural integrity, ensures load-bearing capacity, reduces stress concentration, and simplifies construction [1,2]. Numerous researchers [3–13] have conducted studies on different types of shear walls, which may incorporate window or door openings either

during the initial design or post-construction modifications. As mentioned by Hosseini et al. [3], these openings are the areas of vulnerability in the structural performance, as they can cause stresses that are difficult to predict and may not follow the typical failure modes of the walls without openings, thereby making it challenging to design the structure. Moreover, the rigidity and the structure capacity also may be negatively impacted based on the size of these openings. In general, it is assumed that the impacts of small openings may generally be disregarded. In contrast, large openings typically substantially impact the structural system [4], although no specific description of the size threshold exists in the literature. Constructing openings in concrete structural walls is restricted and governed by the building codes. As an example, the American Concrete Institute (ACI) 318-2019 [5] recommends that seismic hooks or U-bars should be used to terminate reinforcing steel bars in reinforced concrete walls that have been removed to make openings.

There have been several studies conducted in recent years on shear walls, particularly regarding the guidelines for creating openings in these elements. Liu et al. [6] conducted an experimental and theoretical investigation to determine how post-opening location affects the seismic performance of reinforced squat shear walls. The post-opening faults at the center, bottom, and top of the structure were simulated by constructing four RC walls. This research showed that flexural shear failure occurs in both shear walls with no openings and reinforced shear walls with a single post-opening, with the difference in bearing capacity between the two types of specimens being within 6%. Furthermore, finite element analysis (FEA) revealed that the inclusion of a steel plate significantly reduces the uneven distribution of reinforcement strains around the opening in shear walls at different post-opening positions.

Mosoarca [7] presented the theoretical and experimental studies for five wall samples exposed to seismic loads to evaluate and contrast the failure modes in response to earthquakes for three specific categories of shear walls made of reinforced concrete. The failure modes have been determined using calculus software and cyclically alternating experimental investigations. According to the findings, walls featuring staggered openings are sturdier and possess higher load-bearing capacity than walls with regular openings, even when reinforced with the same amount of materials. As a result, these walls can endure seismic forces and horizontal displacements 11.6% better than walls with standard openings before collapsing [7]. Popescu et al. [8] carried out practical studies to explore the impact of various openings on big concrete wall panels' axial strength. A consistent axial load with a small amount of eccentricity was applied to three one-half-scale walls, wherein two opening configurations, one for a little door and one for a huge door, were examined. The findings demonstrated that both large and small openings diminished the solid wall's cross-sectional area by 50% and 25%, respectively, causing a decrease in loading capacity by approximately 50% for large openings and 36% for small openings. The specimen with the smaller opening was generally more rigid than the larger one.

Li et al. [9] experimented to study how the size, placement, and irregularity of openings influence the seismic behavior of shear walls. During the experimental phase, six shear walls with openings and flanges were evaluated under quasi-static side loading. The findings revealed that openings located close to the border or perimeter of the walls might weaken their rigidity and strength. However, the openings may have little effect on their deformation capacity. Additionally, the experiment showed that the larger the aperture, the greater the loss of strength and stiffness. Moreover, incorporating flanges could considerably boost ultimate strength while decreasing deformation capabilities. Mosallam et al. [2] analyzed the structural behavior of five walls of reinforced concrete exposed to a combination of two conditions of sustained compression in the axial direction and periodic lateral loading through an experiment. The research verified that the openings' shape, size, and position affected the modified walls' flexibility and strength characteristics. The study showed that RC walls with openings had lower structural capacity compared to walls without openings. The maximum loads of the unreinforced shear wall with an

off-center door opening and a central window opening were around 13% lower than those of the solid control wall.

Aslani et al. [1] constructed a nonlinear finite element model to study the impact of openings with varying sizes and positions in nine walls of reinforced concrete. The finite element models of reinforced concrete (RC) walls with openings were developed using the ABAQUS software (Version 6.10) [10]. The FE findings demonstrated that opening decreased the loading capacity, stiffness, and the ability of the walls to absorb energy while increasing their displacement. The best opening location in the wall to obtain the maximum load capacity is at its center, and it is suggested that the opening shift to the anchor on the wall; this reduces the wall's ultimate bearing capacity. Furthermore, there is a decrease in tensile damage to the wall as the opening size rises and the ultimate bearing capacity decreases. Hosseini et al. [3] conducted an assessment of the structural behavior of three shear walls of reinforced concrete that had been modified by cutting out openings, emphasizing increasing the eccentricity of the openings. The walls were subjected to cyclic loading in reverse. The findings indicated that eccentric openings improved the flexibility of short shear walls. In addition, the study revealed that creating openings significantly decreased the wall's absorption capacity dissipated energy by reducing its ability to absorb and dissipate energy resulting from loading or impact without experiencing failure or collapse, and subsequently reduced its capacity to resist lateral loading. Ou et al. [11] investigated the impact of various window sizes and locations through controlled experimentation. They used lateral cyclic loads to test five squat RC walls with openings that are common in the outside walls on the backside of first-story row buildings in Taiwan. According to the test results, when comparing walls with openings in the middle and on the edge of the wall web, the mean lateral strength of the side wall was greater. The lateral strength was diminished more by the increase in the opening length than by the rise in the opening height.

Yu et al. [4] experimentally examined the impact that small openings have on the strength of reinforced concrete walls. Periodic lateral loading was applied to five walls with small openings and an aspect percentage of 2.60. Flexural yielding was observed in all the tested samples, and the investigation demonstrated that both bending rigidity and plasticity were unaffected by the tiny opening sizes. According to findings, the flexural conduct of slender walls is unaffected by tiny holes if the walls have adequate shear resistance and the openings are positioned outside of the high-levels-of-compression side and in the region of compression where the stress caused by compression does not diminish. Sabau et al. [12] analyzed the influence of openings on the structural response of multiple-story reinforced concrete (RC) buildings through finite element analysis. The results demonstrated that introducing cut-out openings in the RC load-bearing wall systems of multi-story buildings significantly reduces their resilience. The structures are initially sturdy. Thus, large cut-out openings can be constructed without requiring structural reinforcement under normal service conditions.

Todea et al. [13] examined the seismic response and effectiveness of steel–concrete paired walls using standard reinforcing coupling beams and regular openings by conducting an experimental investigation on five concrete walls exposed to vertical and periodic lateral loads. Their findings showed that the loss of ductility caused by openings could be recovered and greatly enhanced by inserting additional steel fibers in the concrete matrix. The composite wall's web panel is made of steel and concrete, and the link between the two materials is designed to last until the specimens collapse completely according to the study. However, the solid walls' loading capacity was reduced by over 75% due to large openings (which made up 21% of the total wall area).

Based on previous review studies, it is clear that understanding the impact of openings and their sizes in reinforced concrete walls on load-bearing capacity is crucial. By examining the optimal locations for these openings and proposing practical applications, the behavior of concrete walls under vertical and lateral loads can be better predicted. This approach will minimize the need for excessive reinforcement around openings and allow

structural designers to consider the effects of these modifications during the design phase. Additionally, it will help us identify the least detrimental locations for openings, preserving the wall's load-bearing capacity. Therefore, a detailed analysis of factors such as opening placement and size, wall aspect ratio, axial load, and concrete strength is essential to bridge the gap between theoretical models and real-world applications.

2. Finite Element Modeling

ABAQUS Standard 6.14, a commercial finite element software, was used to develop the numerical simulations of reinforced concrete shear walls. The material and geometric nonlinearities were adopted in the proposed FE model. Additionally, the developed models were used to assess the impact of various parameters—such as opening location and size, wall aspect ratio, axial load, and concrete strength—on the performance of shear walls.

2.1. Element Types and Meshing

The nonlinear FE model was developed using the ABAQUS software version 6.14 [10] to simulate the specimens. The type of element used to simulate the concrete and steel sheets was the C3D8R, which is a brick element consisting of eight nodes and three degrees of freedom is utilized for translational movement at every node. To represent the steel reinforcement, two-node truss elements were utilized, and each node of these elements had three degrees of freedom for translational movements (T3D2) [10]. Embedded region constraints were established to model the interaction between the truss elements and the surrounding concrete. In this setup, the steel reinforcement elements were defined as the embedded regions, while the concrete elements served as the host regions. The elements' sizes were selected to be less than 50 mm to reduce the calculation times and the convergence issues [14,15]. The FE meshing of the two parts is illustrated in Figure 1.

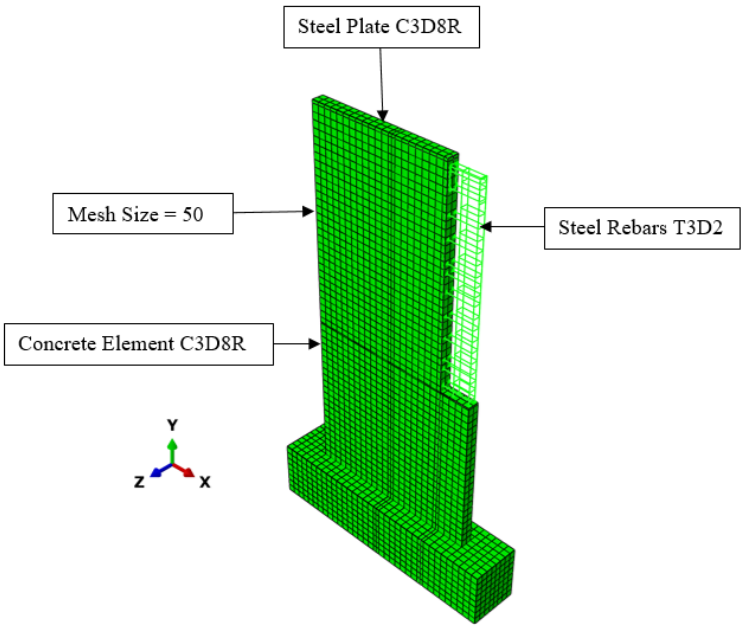

Figure 1. Finite element mesh of the model.

2.2. Material Constitutive Modeling

ABAQUS's [10] material library includes the concrete damaged plasticity (CDP) model which is employed to simulate the mechanical response of concrete after it has been damaged. This model was employed to represent concrete's nonlinear behavior. This model considers that the two primary concrete failure mechanisms, tensile cracking, and compressive crushing, may occur. For the CDP model, materials require a stress–strain relationship that changes with the values of stress and inelastic strain applied to them.

According to Kabaila et al. [16], the relationship between the compressive stress of concrete σ_c and the corresponding strain ε_c can be developed as follows:

$$\sigma_c = \left[\frac{E_c \varepsilon_c}{1 + (R + R_E - 2)\left(\frac{\varepsilon_c}{\varepsilon_o}\right) - (2R - 1)\left(\frac{\varepsilon_c}{\varepsilon_o}\right)^2 + R\left(\frac{\varepsilon_c}{\varepsilon_o}\right)^3} \right] \quad (1)$$

where $\varepsilon_0 = 0.0025$, $R_E = 4$, and $R_\sigma = 4$, where ε_0 is the strain at the peak stress and R, R_E, and R_σ are the parameters depending on concrete properties using the criteria established by Hu and Schnobrich [17]; f'_c is the compressive strength of concrete; E_c is the elastic modulus; and E_0 is the initial elastic modulus, as determined by (ACI 318-19) [5].

$$\mathrm{R} = \frac{\mathrm{R_E}(\mathrm{R_\sigma} - 1)}{(\mathrm{R_E} - 1)^2} - \frac{1}{\mathrm{R_E}} \quad (2)$$

$$R_E = \frac{E_c}{E_o} \quad (3)$$

$$E_o = \frac{f'_c}{\varepsilon_o} \quad (4)$$

$$E_c = 4700\sqrt{f'_c} \quad (5)$$

The elastic modulus, determined in Equation (5); Poisson's ratio of 0.2; and the characteristics of plasticity are the three quantities needed for the CDP model. Table 1 summarizes the plasticity parameters that the CDP model in ABAQUS requires. The only value that differs is the dilation angle, which was determined by [18,19]. The Viscosity parameter was taken to be small enough to not affect the reliability of the results.

Table 1. The characteristics of the plasticity parameters.

Dilation Angle (ψ)	Eccentricity	f_{bo} / f_{co}	*K*	Viscosity Parameter
37	0.1	1.16	0.67	0.001

In uniaxial tension, concrete is anticipated to exhibit tension-stiffening behavior that mirrors its tensile behavior after cracking. It is assumed that concrete has a linear elasticity up to its tensile cracking strength (f_{cm}), after which strain softening occurs. Stress vs. cracking strain is used to determine the post-cracking behavior. The model for tension stiffening developed by Nayal and Rasheed [20] was utilized. The concrete's nonlinear conduct in response to uniaxial tension and compression is illustrated in Figure 2.

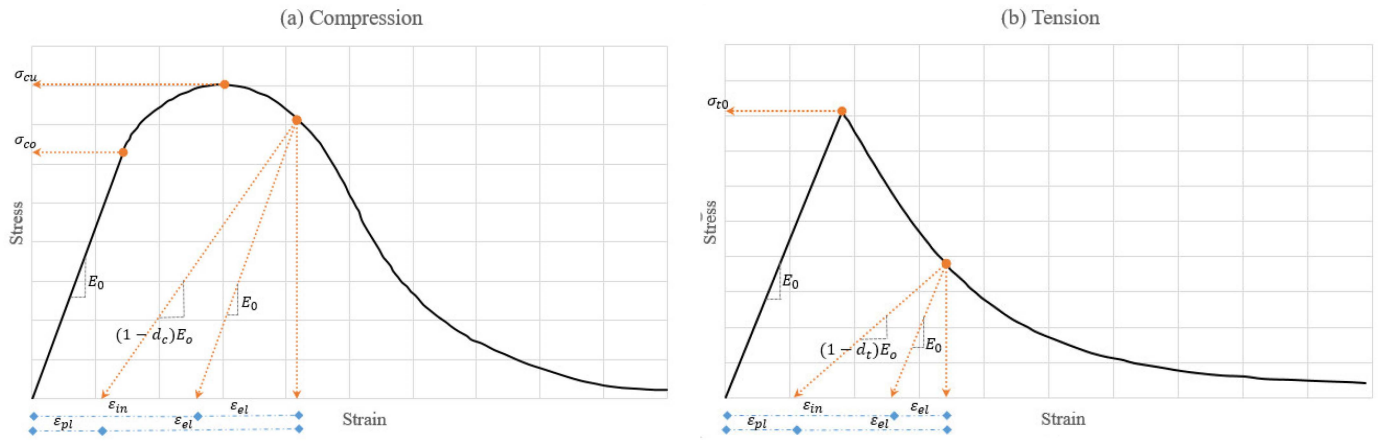

Figure 2. The response of the concrete subjected to uniaxial stress for the CDP model (**a**) Compression and (**b**) Tension.

Creating damage variables d_t and d_c in ABAQUS [10] is a necessary step in the CDP model, which simulates the reduction in concrete stiffness under a constant force. As a part of this study, the parameterization of damage variables in compression and tension, d_c and d_t, respectively, was characterized using a linear damage parameter–strain equation. The two damage variables, d_c and d_t, are 0.90, and are expected to reach a maximum value of 0.90, which stands for the complete degradation of the concrete material [7]. The CDP model defines perfectly plastic behavior as a function of inelastic strain and yield stress. It has not been impacted if the concrete remains intact after approaching the softening range. At $\varepsilon_t > \frac{\sigma_t}{E_c}$, the slope of E_c is equivalent to the unloading trajectory of the stress–strain curve, and the corresponding strain is caused by elasticity $\left(\varepsilon_{t,d}^{el} = \frac{\sigma_t}{E_c}\right)$, where σ_t refers to the concrete's tensile stress. If cracking causes damage to the concrete, the unloading trajectory's slope is decreased to $(1 - d_t)E_c$; also, the strain due to elasticity is $\varepsilon_t^{el} = \left(\frac{\sigma_t}{[(1-d_t)E_c]}\right)$, where d_t represents the damage factor for tension in damaged concrete. The definition of the cracking strain for damaged concrete in ABAQUS [10] is based on Equation 6, which was proposed by Lubliner et al. [21]:

$$\varepsilon_t^{cr} = \varepsilon_t - \varepsilon_t^{el} \tag{6}$$

The equivalent plastic strain can be summed up as follows for concrete that has undergone damage:

$$\varepsilon_t^{pl} = \varepsilon_t - \varepsilon_{t,d}^{el} \tag{7}$$

Birtel and Mark [22] offer the damage parameter for the concrete under compression employed in the suggested model.

$$d_c = 1 - \frac{\sigma_c E_c^{-1}}{\varepsilon_c^{pl}\left(\frac{1}{b_c} - 1\right) + f_c E_c^{-1}} \tag{8}$$

where d_c is a damage parameter for concrete under compression, f_c is the compressive stress, E_c is concrete's elasticity modulus, ε_c^{pl} is the plastic strain corresponding to compressive strength, and b_c is the constant range $0 < b_c < 1$, whereas the criterion for concrete tension damage is proposed by Birtel and Mark [22] as follows:

$$d_t = 1 - \frac{\sigma_t E_c^{-1}}{\varepsilon_t^{pl}\left(\frac{1}{b_t} - 1\right) + f_t E_c^{-1}} \tag{9}$$

where d_t is the damage parameter for concrete under tension, f_t is the tensile stress, E_c is concrete's elasticity modulus, ε_t^{pl} is the plastic strain corresponding to tensile strength, and b_t is the constant range $0 < b_t < 1$.

In this model, steel reinforcement is assumed to display elastic–perfectly plastic behavior and was employed to simulate its response under tension and compression. This is a logical assumption for reinforcing steel bars. It is widely used by other researchers in nonlinear finite element analysis employing the ABAQUS FE program [10]. Steel reinforcing properties are mentioned in Table 2, knowing Poisson's ratio of 0.3.

Table 2. Material properties of the RC shear wall model.

	Average Tensile Strength [MPa]	**Average Compressive Strength [MPa]**	**Compressive Strain**	**Modulus of Elasticity [MPa]**
Concrete	$F_{ctm} = 3$	$F_{cm} = 50$	0.0035	$E_c = 34{,}000$
	Diameter [mm]	**Yield Strength [MPa]**	**Ultimate Strength [MPa]**	**Modulus of Elasticity [MPa]**
Rebar	6	$F_y = 386$	$F_u = 551$	$E_s = 210{,}000$

2.3. Boundary Conditions and Interaction Properties

Finding a method of interaction between the concrete surfaces was crucial to finishing the construction of the FE model. There are two different types of interactions that need to be characterized. Firstly, the interaction between the concrete surfaces was first created as a tie-constraint alternative. Second, an embedded zone was designed to imitate an excellent bond between the steel rebars and the cement components. Also, to apply the lateral load on the model's top surface, a reference point (RP) was used and connected to the wall as a coupling restriction. The samples were subjected to monotonic loading in the lateral direction and axial compressive force. Figure 3 shows the loading and boundary conditions of the FE model. By post-tensioning the specimen's foundation to the solid base and simulating it as an enclosure boundary condition, the specimens were attached to a sturdy floor.

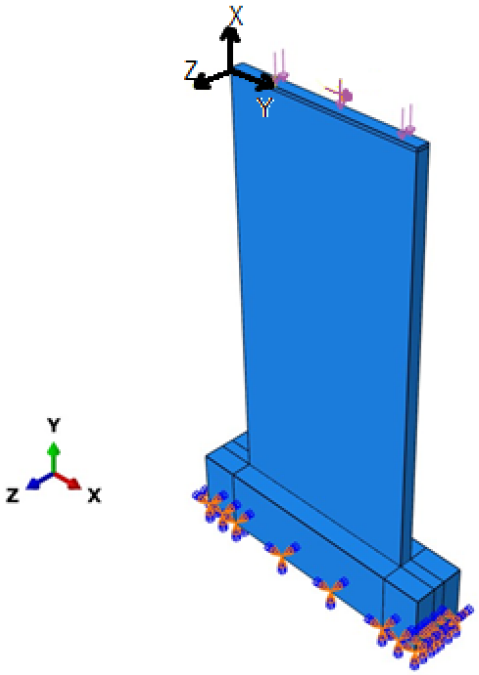

Figure 3. Loading and boundary conditions of the CW specimen.

3. Model Verification

3.1. Previous Experimental Work

An experimental study available in the literature and performed by Mosoarca [7] was used to check the precision of the numerical model constructed in the current study. In this study, five shear wall samples SW1, SW23, SW45, SW67, and SW8 were selected to be simulated through FE modeling. The specimens tested included three with zigzag openings (SW23, SW45, and SW67), one with consistent openings (SW8), and one with no openings (SW1). The purpose of the test was to determine wall failure modes, and the specimens were constructed at a 0.25 scale. The specimens were securely bolted to the structural floor and tested in a vertical orientation, as illustrated in Figure 4. A cyclic lateral load was applied at the top using a hydraulic actuator, which operated in displacement-controlled mode. Figure 4 shows the experimental configurations, the wall dimensions, and the wall reinforcing details.

The geometric dimensions and reinforcing patterns of these samples are identical. The wall specimens' dimensions were 2600 mm, 1250 mm, and 80 mm in height, length, and wall thickness, respectively. The reinforcements for both bending and shear on both sides of the wall comprised a 6 mm diameter rebar. The aspect ratio of these specimens is approximately 2. The specimens comprised three main parts: a U-shaped steel plate that transferred lateral loads to the wall, the wall panel itself, and a footing used to anchor the

specimen to the solid floor for stability. Lateral supports were used to limit the degree of motion that restricts moving out of a plane. The concrete utilized in this research had an average compressive strength of 50 MPa. Table 2 summarizes the mechanical parameters of the reinforced rebar and concrete. The experimental protocol consisted of two stages of loading. The first stage involved applying a constant axial force of 50 kN on the top surface of the wall, followed by the second stage, which included the application of a horizontal lateral load on the top surface using the protocol for displacement control. A sturdy steel plate (with a thickness of 25 mm) was attached to the top surface of the wall specimens, where loads were applied horizontally and vertically to spread the load and avoid any stress concentration.

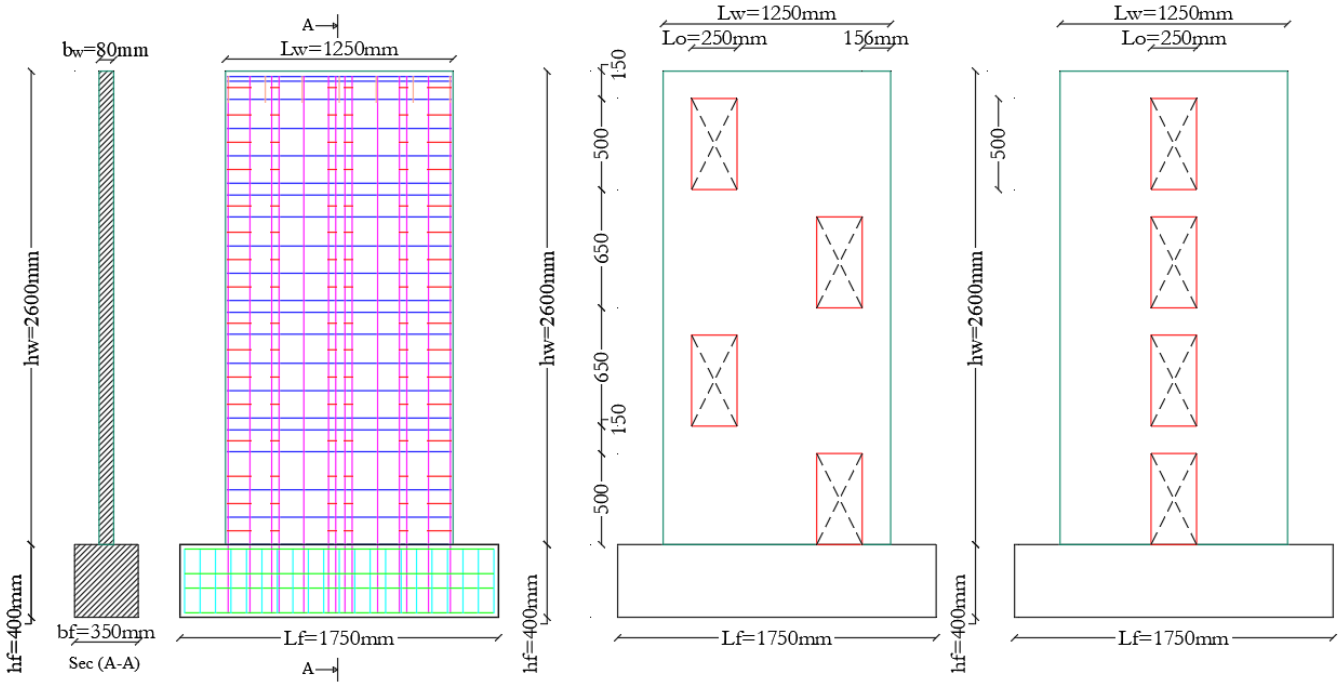

(**a**) SW1 (**b**) SW23, SW45, and SW67 (**c**) SW8

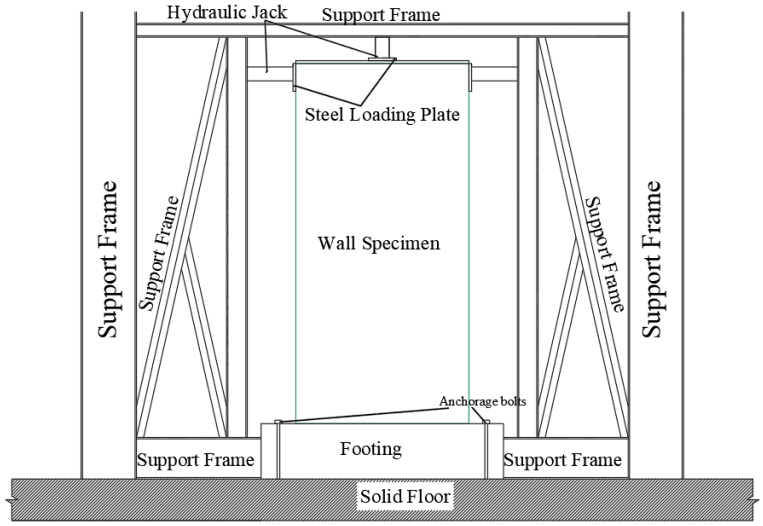

(**d**) Loading scheme

Figure 4. Experimental setup and reinforcing steel.

3.2. Verification of the FE Results

In general, to validate the suggested FE model, Mosoarca's [7] experimental test results have been compared to the predicted FE results. The FE models had a quarter-scale size as mentioned by Mosoarca [7] where these models represented 4-story rectangular walls in reality. All the specimens were tested under two loading stages: a constant vertical axial force (50 kN) is first applied on the top surface of the wall, and then the horizontal lateral load is imposed on the top through a displacement control protocol. The horizontal load was applied in a monotonic increasing way on the top of the wall. The bottom footing was used as a fixed support to the bottom surface of the shear wall. The lateral load–displacement curves were used to compare the experimental data with the results of the finite element analysis and the damage failure modes of the analytical and experimental specimens were presented through figures and tables. The subsequent sections illustrate the validations of the FE results.

3.2.1. Load–Displacement Response

Figures 5 and 6 present a comparison between the curves of lateral load versus top displacement relationships obtained from the FE model with the experimental findings of Mosoarca [7]. It can be observed that the numerical results correspond closely with the experimental data. The FEM and experimental curves exhibited identical pattern behaviors, as shown in Figures 5 and 6. For the solid control wall (CW), the maximum load capacity observed experimentally was 113.63 kN. In comparison, the FE analysis yielded a value of 106.40 kN, which corresponds to 93.63% of the experimental result. Table 3 displays the expected final lateral loads and displacements by the FE analysis for the walls CW and SW8.

Table 3. Comparing the numerical and experimental outcomes [7] for all the samples.

Specimens Label	Experimental [5]		Numerical (FEM)		PFEM/PEXP %
	Ultimate Load PEXP [kN]	Ultimate Displacement [mm]	Ultimate Load PFEM [kN]	Ultimate Displacement [mm]	
CW	113.63	14.00	106.397	26.48	93.63
SW8	70.85	11.80	68.80	13.60	97.10

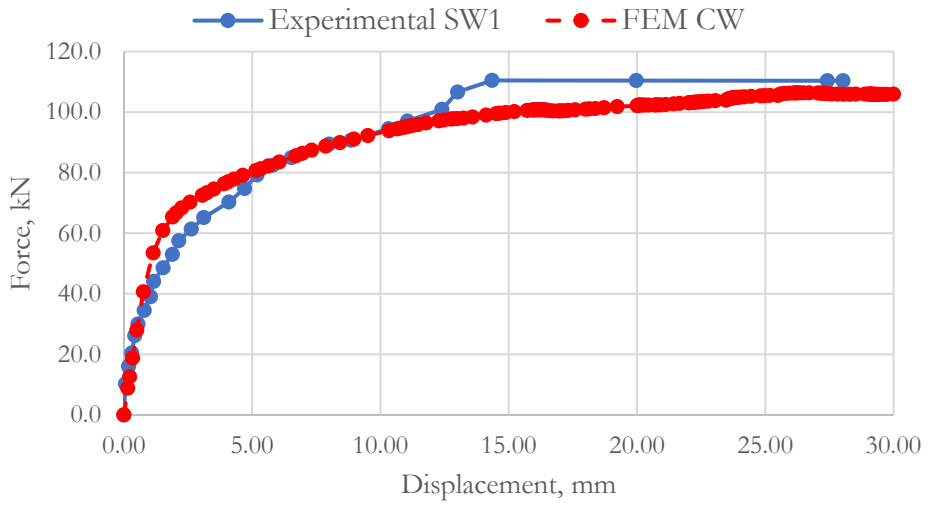

Figure 5. The relationships of the FE analysis versus experimental analysis for the control wall specimen.

Based on the information presented in Table 3, it was noted that the RC walls with openings had lower structural strengths than those without openings. Wall specimen SW8's maximum capacity of lateral load decreased by 37.6% in comparison to the control wall.

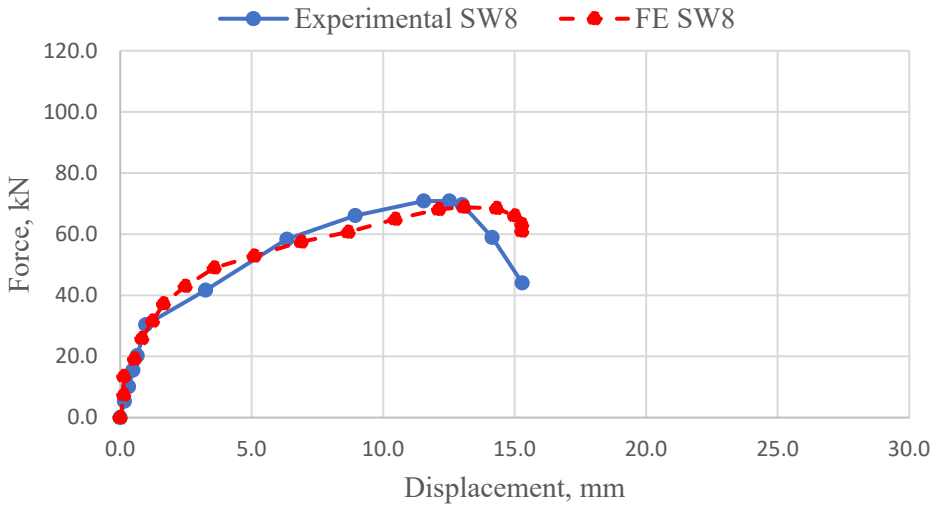

Figure 6. Force versus displacement curves for experimental and numerical analysis of SW8.

3.2.2. Crack Patterns and Failure Modes

As observed in Figures 7–9, the failure modes of the wall specimens acquired experimentally by [7] were compared to those obtained using the FE software (ABAQUS, Version 6.10). These modes of failure are determined by examining the contours of the highest primary strains present at the mid-surface. The shear wall specimens exhibited various failure modes, such as flexural cracks in the tension zone, crushed concrete at the wall base, and the yielding of steel reinforcement on the side of tension. The control sample, designated as CW, experienced failure due to flexural stress, although the initial fracture was noticed towards the wall's footing in the tensile zone at a lateral force of 54.4 kN. For specimen SW8, bending cracks form towards the piers' footing, where the initial crack was discovered at a lateral load of 13.50 kN.

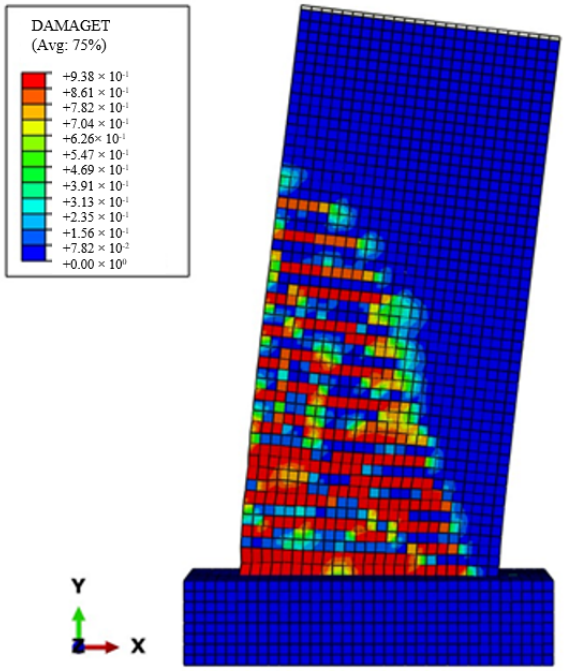

Figure 7. The damage mode of the concrete failure of the FE analysis for the FEM CW model.

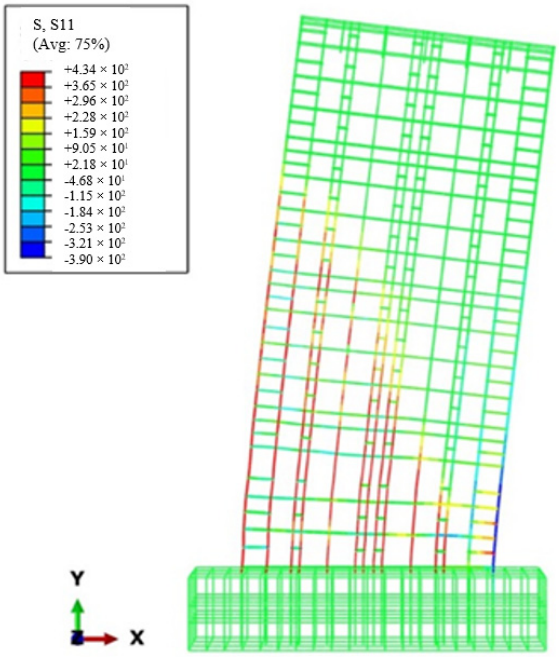

Figure 8. The steel reinforcement yielded at the point of failure load for the CW specimen.

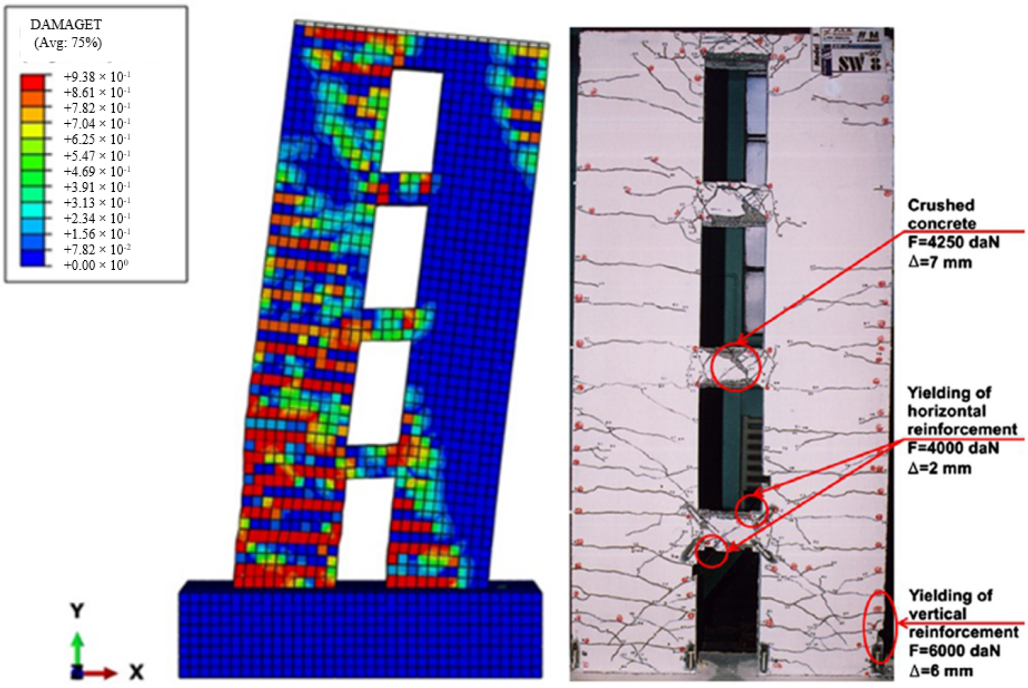

Figure 9. The failure mode of concrete damage in the FE analysis for the SW8 model.

4. Parametric Study

In this part, the following five parameters were investigated and analyzed: the cutting-out opening locations on the wall, the ratio of the opening size to the wall, the aspect ratio of the shear wall, the different axial loads with constant lateral load, and the concrete strength. These parameters significantly impact the structural strength of the RC walls with openings. The identical CDP model was constructed for each example to assess the conduct of the wall. The five parameters' influences on the strength of the wall are discussed in the subsequent sections. Table 4 and Figure 10 depict the geometric details of the shear walls and the arrangement and locations of the openings for parametric study no (1 and 3), which is related to the effect of opening locations and the aspect ratios of the walls, respectively.

In this research, the specimens and locations of the openings were labeled using specific notations: "SW" means shear wall with an opening, "CW" means control wall without an opening, "e" means eccentricity ratio, "No" means wall without opening, "B" means wall with bottom opening, "M" means wall with middle opening, "T" means wall with top opening, "R" means the proportion of the opening area to the wall's area, "AR" means the aspect ratio of the wall, "P" means axial load value, and "f_c'" means concrete compressive strength value.

Table 4. Brief description of the FE parametric analysis for the wall specimens.

Parametric Study	Opening Location	Specimen Label	Dim. of Wall hw × lw × bw [mm, mm, mm]	Opening dim. and loc.		
				a × b [mm]	X [mm]	Y [mm]
Parametric no (1) locations of cutting-out openings P = 750 kN and f_c' = 50 MPa	No	CW	2600 × 1250 × 80	-----	0	0
	B	SW1-e0%		500 × 1000	625	500
		SW2-e8%		500 × 1000	525	500
		SW3-e16%		500 × 1000	425	500
	M	SW4-e0%		500 × 1000	625	1300
		SW5-e8%		500 × 1000	525	1300
		SW6-e16%		500 × 1000	425	1300
	T	SW7-e0%		500 × 1000	625	2100
		SW8-e8%		500 × 1000	525	2100
		SW9-e16%		500 × 1000	425	2100
Parametric no (3) aspect ratios of shear walls P = 750 kN and f_c' = 50 MPa	No	CW-AR0.5	625 × 1250 × 80	-----	0	0
	No	CW-AR1	1250 × 1250 × 80	-----	0	0
	B	SW1-AR1		500 × 1000	625	500
	M	SW4-AR1		500 × 1000	625	625
	T	SW7-AR1		500 × 1000	625	750
	No	CW-AR1.5	1875 × 1250 × 80	-----	0	0
	B	SW1-AR1.5		500 × 1000	625	500
	M	SW4-AR1.5		500 × 1000	625	937.50
	T	SW7-AR1.5		500 × 1000	625	1375
	No	CW-AR2	2600 × 1250 × 80	-----	0	0
	B	SW1-AR2		500 × 1000	625	500
	M	SW4-AR2		500 × 1000	625	1300
	T	SW7-AR2		500 × 1000	625	2100
	No	CW-AR3	3850 × 1250 × 80	-----	0	0
	B	SW1-AR3		500 × 1000	625	500
	M	SW4-AR3		500 × 1000	625	1925
	T	SW7-AR3		500 × 1000	625	3350

Table 5 shows a comparison between the real-life dimensions and the FE parametric study. A quarter-scale model of the wall was utilized to simplify the finite element (FE) model and control the increase in nodes and elements. These scaled-down models functioned as simulation tools, offering insights for the full-scale wall models and predicting the behavior of various specimens under specified conditions. The proposed openings were strategically positioned to accommodate architectural features such as doors, windows, air conditioners, and elevator doors, as well as to replicate the random cuts that typically occur in practice due to workers' limited understanding of the structural behavior. Lateral supports were used to constrain the out-of-plane degrees of freedom in all the analyzed models. The walls were reinforced with two layers of steel rebars, with a concrete cover of 15 mm.

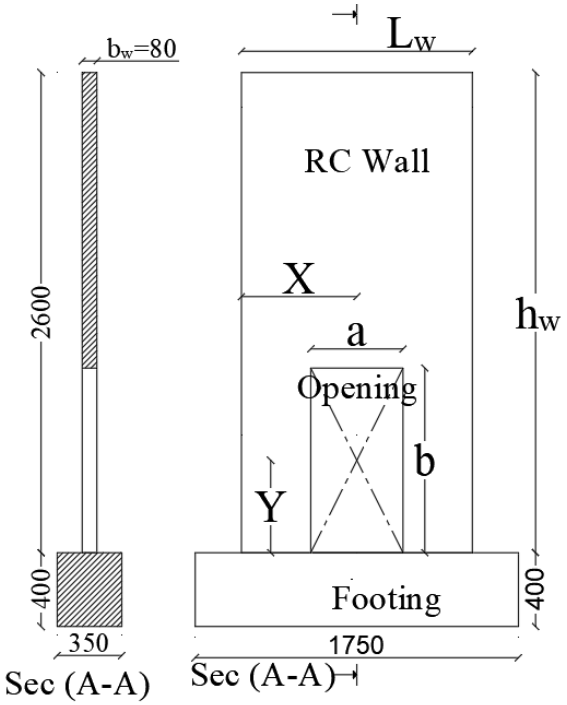

Figure 10. The geometry of the wall and specimen details (all dimensions in mm).

Table 5. Comparisons of the real-life dimensions and the FE parametric study.

Dimension	Shear Wall Real Life (mm)	Numerical Model (mm)
Wall height	10,400	2600
Wall width	5000	1250
Wall thickness	250	80
Opening height	2000	500
Opening width	1000	250

4.1. Methodology of Changing Cutting-Out Opening Locations in the Shear Wall

Openings are made in various locations in a wall due to the architectural constraints to comply with updated changes or satisfy modern living requirements. Hence, in this parameter, nine specimens SW1–SW9 with openings were studied by fixing the dimensions of the walls and openings and changing the locations of the openings; the opening size was selected to represent the best cutting-out opening locations in the shear wall to obtain the strongest load capacity as mentioned by Hosseini et al. [3]. The RC wall specimen dimensions were used, which were the same specimen dimensions used in the verification part. The nine samples are detailed in Table 4 in the section of parametric study no 1 where each sample differs from the others in the level of cutting in the wall and the eccentricity ratio. In the shear walls, the eccentricity ratio is measured between the center line of the opening and the center line of the wall horizontally. The values for this eccentricity are illustrated in Figure 11. According to design codes such as [23], if the opening's height is greater than 1/3 of the total wall's height, it will be influential in terms of results.

Moreover, Wang et al. [24,25] mentioned that the experimental parameter used for the opening ratio is 0.46, and its definition is given as follows: $\eta = \sqrt{\frac{h_o l_o}{h_w l_w}} \leq 0.46$, where h_o and l_o are the opening's height and length, respectively. The variable h_w refers to the clear wall's height between the beams, measured from their centers. Meanwhile, the variable l_w represents the distance between the two side columns, also measured from their centers. The specimens were designed to withstand a constant vertical axial force of 750 kN, which

resulted in a mean compressive stress of 0.5 N/mm^2. In addition, a static horizontal load was applied on the top of each sample using a displacement control protocol.

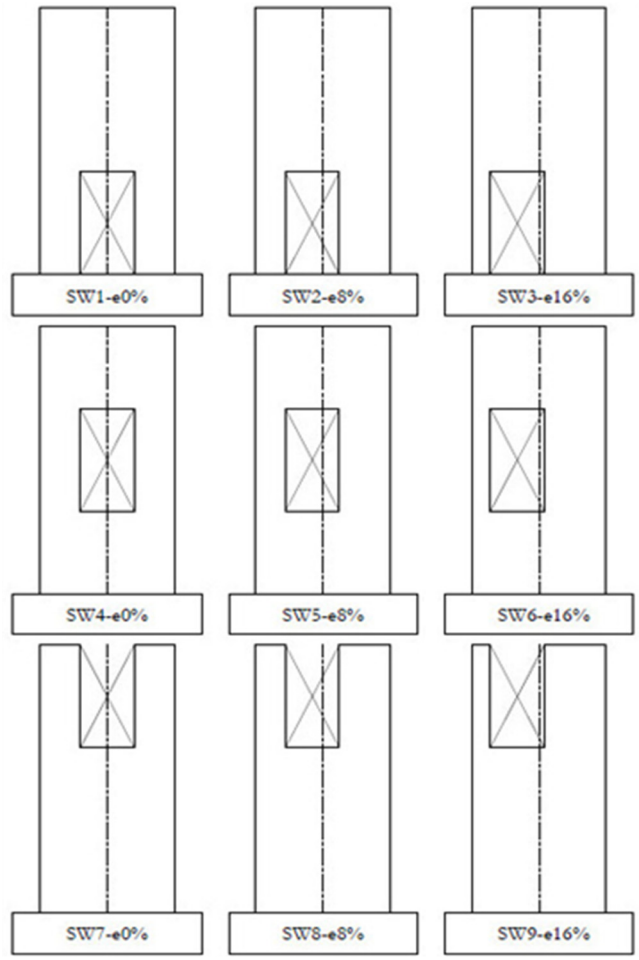

Figure 11. Designed RC shear walls SW1-SW9.

4.2. Effect of Changing the Cutting-Out Opening Locations

The position of the opening and the degree of eccentricity can significantly impact the shear strength of a structural wall made of reinforced concrete. Specifically, relocating the opening from the bottom to the top of the wall and increasing the eccentricity can have a strong influence on the wall's loading strength. Figure 12 displays the force–displacement curves for the wall specimens with openings. These figures indicate that the location of the opening effectively affects the load-bearing strength of the concrete wall; the closer the opening is to the wall support (the footing) at the bottom of the wall, the load-bearing capacity of the wall decreases by 24.4%, unlike in the case of the opening at the top of the wall as illustrated in Figure 11, where the decrease in the loading strength of the wall reaches to 4.8%. Hence, the farther the opening is from the wall support, the better the percentage of decrease in wall strength in comparison to the control wall with no openings. It was also summarized that the ratio of the eccentricity of the opening from the center of the wall dramatically affects the wall strength according to the opening level in the wall. That is, as the opening deviation ratio from the wall center axis at any location on the wall increased, the enhanced rate of reduction in wall capacity increased from 24% to 18%. In summary, the optimal location for the openings cut in the wall should be away from the wall center axis and the wall support.

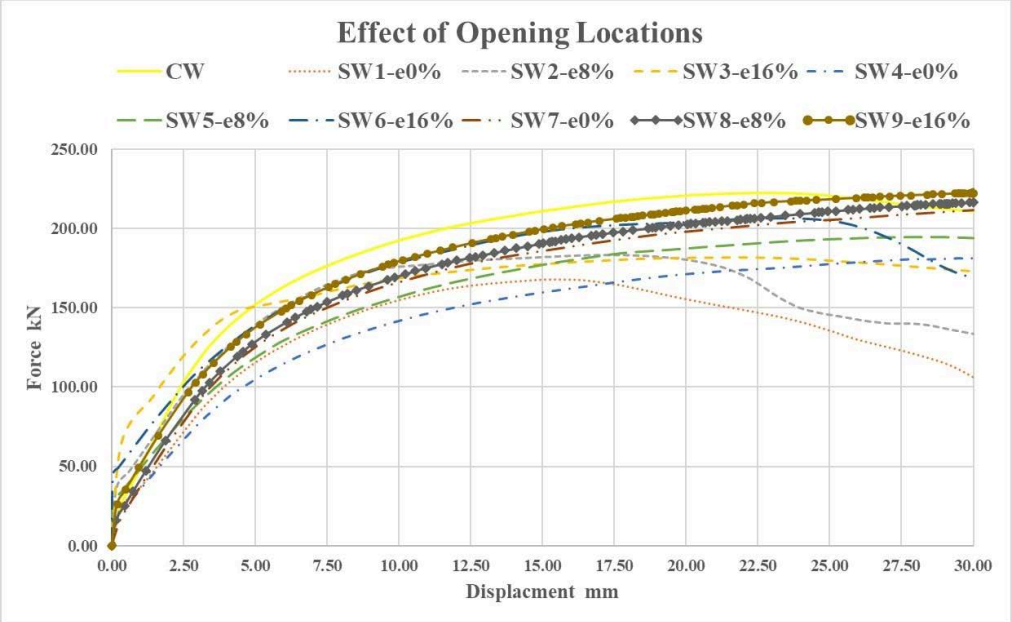

Figure 12. Force–displacement curves for wall specimens SW1–SW7.

As can be seen in this figure, the location of the opening is affected by how close the opening is to the base of the wall. Comparing the curves in Figure 12 demonstrate how much of a decrease in the loading strength of the wall increases by cutting openings near the wall's base and vice versa with openings at the top of the wall away from the wall's base. In light of these findings, it is possible to deduce that SW3-e16% exhibited the most favorable performance in terms of the loading capacity compared with SW1-e0% and SW2-e8%, and also SW9-e16% exhibited the most favorable performance among the rest of the specimens. Table 6 provides an overview of the ultimate load % decreases brought on by altered opening locations.

Table 6. Numerical results for wall specimens "SW1–SW9" compared to control wall "CW".

Model Label	Ultimate Load [kN]	Ultimate Displacement [mm]	Percentage Decrease in Ultimate Load
CW	222.3	23.0	0.0
SW1-e0%	168.0	15.2	24.4
SW2-e8%	183.3	17.5	17.5
SW3-e16%	181.8	21.8	18.1
SW4-e0%	181.6	29.8	18.3
SW5-e8%	194.5	28.6	12.5
SW6-e16%	206.5	23.3	7.1
SW7-e0%	211.6	30.0	4.8
SW8-e8%	216.3	30.0	2.6
SW9-e16%	222.3	30.0	0.0

4.3. Effect of Changing the Opening Size

In respect to this parameter, nine samples of RC walls with various opening sizes were studied to investigate the impact of various opening sizes, which is one of the important factors in this study. All the wall specimens in this section have a cross-section area of 1875 mm in height, 1250 mm in length, and 80 mm in thickness, with an aspect ratio of 1.5. The ratio of the dimensions of the wall (1.5) was chosen according to the study shown in the next section regarding the study of the dimensions of a concrete wall with the ratios of 0.5, 1, 1.5, 2, and 3). Hence, from the study, it became clear that the aspect ratio of 1.5 gives the best results in terms of the load capacity. By fixing the dimensions of the RC wall and

changing the sizes of the openings to study the effect of the openings, Table 7 summarizes the nine samples and the dimensions of the openings and shows the proportion of the opening area to the wall area.

Table 7. Opening sizes models compared to the control model.

Model Label	Wall Dimensions [mm]	Opening Percentage	Opening Width [mm]	Opening Height [mm]
CW-R0%	1875 × 1250 × 80	0%	0.00	0.00
SW1-R2%		2.67%	250	250
SW1-R5%		5.30%	250	500
SW1-R10%		10.6%	500	500
SW1-R16%		16%	500	750
SW1-R21%		21.30%	500	1000
SW1-R24%		24%	750	750
SW1-R32%		32%	750	1000
SW1-R42%		42.6%	1000	1000

In general, nine specimens of walls with different opening sizes were modeled, as shown in Figure 13. The concept of experiment and attempt was relied upon to investigate how changing the opening size affects the results through two paths. The first path is fixing the opening's width while changing the opening's height. The second path is fixing the opening height by changing the opening width. The analysis of models was carried out using the compressive strength of concrete f'_c = 50 MPa and the top of the wall was loaded with 750 kN as a constant axial load, and a static lateral load was imposed on the top edge of the analyzed sample through a loading point that was controlled by displacement.

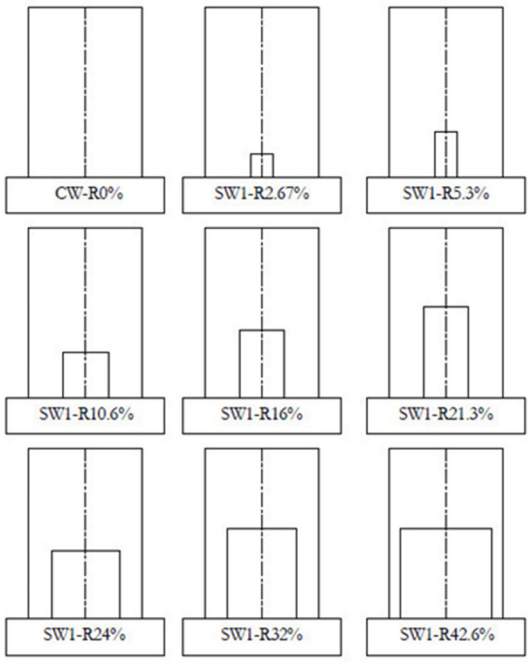

Figure 13. Designed RC shear walls with different opening size percentages.

By using the FEM to analyze these models, it has been observed that the strength of the concrete wall is adversely affected by the width of the opening cut in the wall where different percentages of the openings' sizes were studied, and they are 0, 2.67, 5.3, 10.6, 16, 21.3, 24, 32, and 42.6%. It was found that there is a correspondence between the load curves of SW1-R2% and SW1-R5%, and also between SW1-R10%, SW1-R16%, and SW1-R21% because the width of the opening in both cases is constant. This confirms that

the width of the opening is the critical dimension that greatly affects the behavior of the wall, as shown in Figure 14. Increasing the percentage of openings in the lower part of the wall led to plastic deformation in the steel reinforcement as the concrete was no longer sufficient to maintain stability. As a result, the wall began to destabilize, and negative forces were observed. On the other hand, the other dimension, which is the opening's height, has a slight, unnoticeable effect on the load-bearing capacity of the concrete wall. It was also concluded that with an increase in the ratio of the opening size to the wall area, the load-bearing strength of the wall decreases with the increase in the ductility of the wall. Therefore, it is recommended that any opening in the concrete wall should be reduced, the width should not exceed 40% of the total width, and the area of the cut-out opening should not exceed 21% of the total area of the wall.

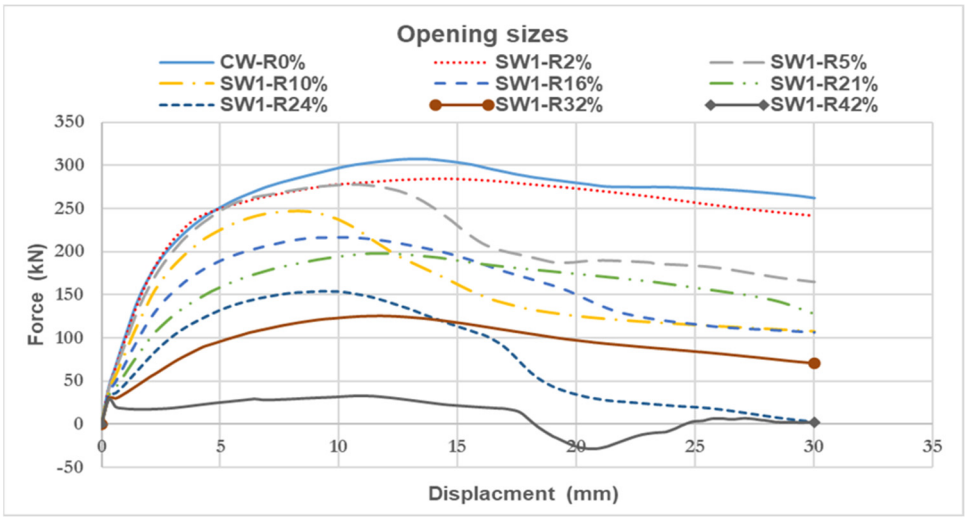

Figure 14. Force-displacement curves for changing the opening size ratios.

4.4. Effect of Changing Aspect Ratios of Shear Walls

For this parameter, seventeen samples were modeled and investigated to study the effect of changing aspect ratios on the behavior of RC shear walls with openings that are subjected to a constant vertical axial force of 750 kN and a horizontal lateral load on the top through a displacement control protocol. These samples were classified into five sets to investigate the numerical models. The details of the analysis are presented as follows: Set a has one specimen of shear walls (CW.AR0.5), which have an aspect ratio of 0.5. Set b has four specimens of shear walls (CW.AR 1, SW1.AR1, SW4.AR1, and SW7.AR1) which have an aspect ratio of 1 and rectangular opening dimensions of 500 mm × 1000 mm at various levels of the bottom, middle, and top of the wall. Set c has four specimens of shear walls (CW.AR1.5, SW1.AR1.5, SW4.AR1.5, and SW7.AR1.5) which have an aspect ratio of 1.5 and rectangular opening dimensions of 500 mm × 1000 mm at various levels of the bottom, middle, and top of the wall. Set d has four specimens of shear walls (CW.AR2, SW1.AR2, SW4.AR2, and SW7.AR2) which have an aspect ratio of 2.08 and rectangular opening (500 mm × 1000 mm) at various levels of the bottom, middle, and top of the wall. Set e has four specimens of shear walls (CW.AR3, SW1.AR3, SW4.AR3, and SW7.AR3) which have an aspect ratio of 3.08 and rectangular opening dimensions of 500 mm × 1000 mm at various levels of the bottom, middle, and top of the wall. The details of the samples studied in this factor are shown in Table 4 in the parametric section no 3 and shown in Figure 15. Also, Table 8 illustrates the details of dividing the samples into five groups and the dimension details of the wall specimens.

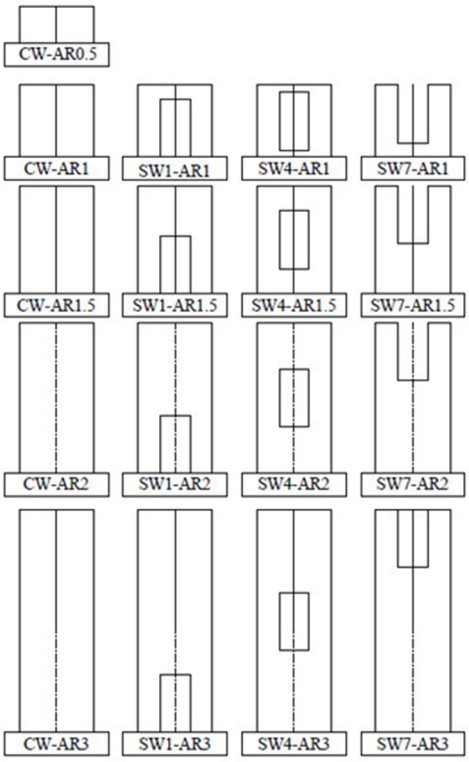

Figure 15. Aspect ratio designed walls.

Table 8. Different aspect ratio models of the walls.

Wall Set	Specimen Label	Dimension $h_w \times l_w \times b_w$ [mm]	Aspect Ratio
Set a	CW.AR0.5	625 × 1250 × 80	0.50
Set b	CW.AR1, SW1.AR1, SW4.AR1, SW7.AR1	1250 × 1250 × 80	1.00
Set c	CW.AR1.5, SW1.AR1.5, SW4.AR1.5, SW7.AR1.5	1875 × 1250 × 80	1.50
Set d	CW.AR2, SW1.AR2, SW4.AR2, SW7.AR2	2600 × 1250 × 80	2.08
Set e	CW.AR3, SW1.AR3, SW4.AR3, SW7.AR3	3850 × 1250 × 80	3.08

In general, the FE analyses' findings showed that by comparing the results of the five sets of control samples with the aspect ratios of 0.5, 1, 1.5, 2, and 3, it is found that increasing the wall aspect ratio (or decrease in slenderness ratio) leads to decreasing the wall's base shear capability. In contrast, the displacement ductility of the structures increases slightly, as illustrated in Figure 16. Also, it was noticed that the differences in the wall capacities for the aspect ratios of 0.5, 1, 1.5, 2, and 3 decreased with the increasing wall aspect ratio by 35%, 30%, 28%, and 35%, respectively. On the other hand, comparing the results in Figure 16b–d found an improvement in the results of the specimens with the aspect ratios of 1.0, 1.5, and 2.0, which means that the opening location leads to an improvement in the difference between the samples. Also, the top opening is the most efficient location to obtain the largest load capacity. Finally, from Figure 16d, it can be concluded that a wall with an aspect ratio of 1.5 is the optimum wall for the shear performance of the RC wall.

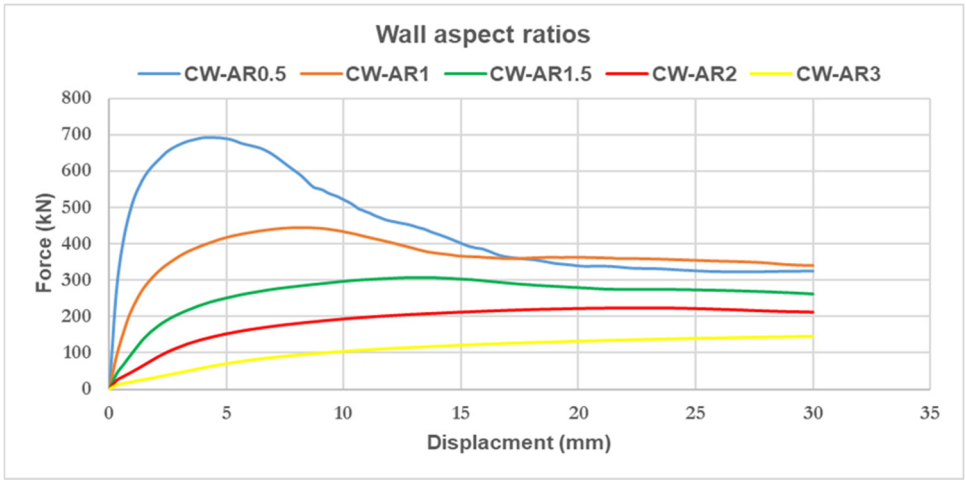

(**a**) Control wall specimens

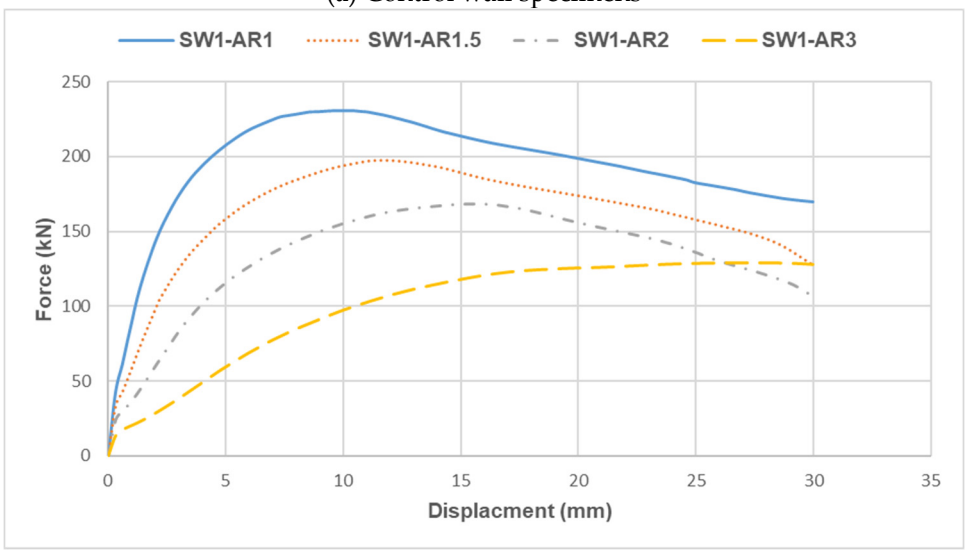

(**b**) Specimens with bottom openings

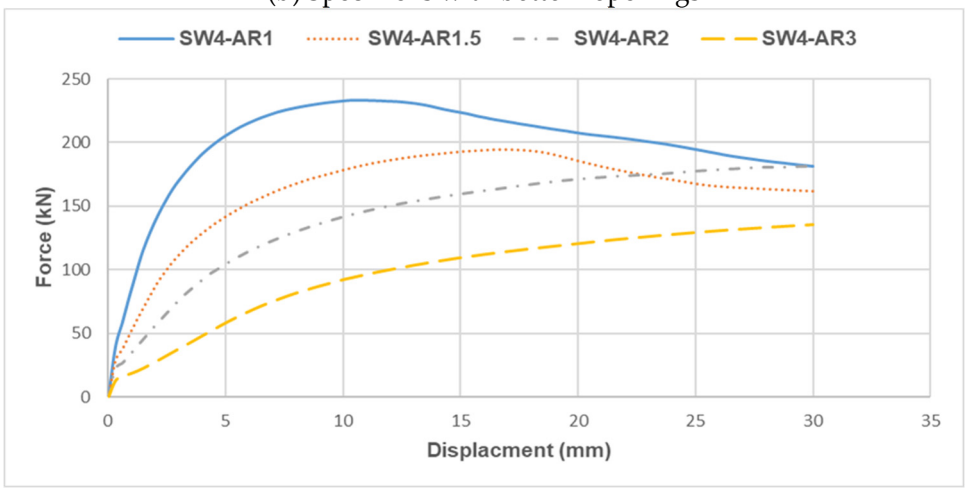

(**c**) Specimens with middle openings

Figure 16. *Cont.*

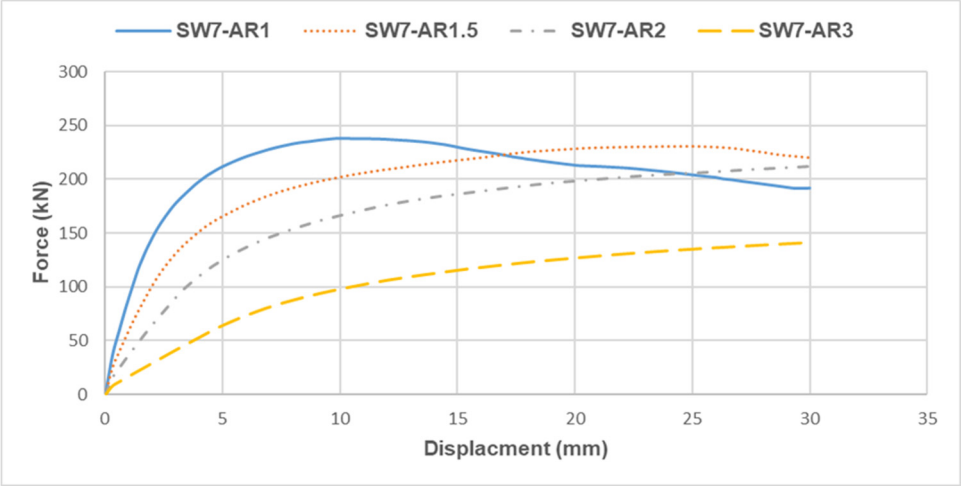

(**d**) Specimens with top openings

Figure 16. The load–displacement curves of the wall specimens with bottom, middle, and top openings.

4.5. Effect of the Vertical Axial Load on Shear Walls

This part of the analysis focuses on examining how variations in the axial load impact the force–displacement curve of the walls. The examined axial load values were 500, 750, and 1000 kN. The effect of the axial load was investigated using the verified model of the control specimen CW with an aspect ratio of 2.0 as listed in Table 4 and shown in Figure 4. The sample studied for this parameter was the same sample used in the verification section. Figure 17 shows the influence of variations in axial load on the walls' ultimate load-carrying capacity. From this diagram, the concrete wall's bearing capacity is enhanced with a rise in the applied axial load. The ratio of increasing wall strength by changing the axial load from 500 kN to 750 kN is about 20%, and 13.5% when the load varies from 750 kN to 1000 kN, as shown in Figure 18. This analysis leads to the inference that with an escalation in vertical load, there is a diminishing rate of enhancement in the wall capacity.

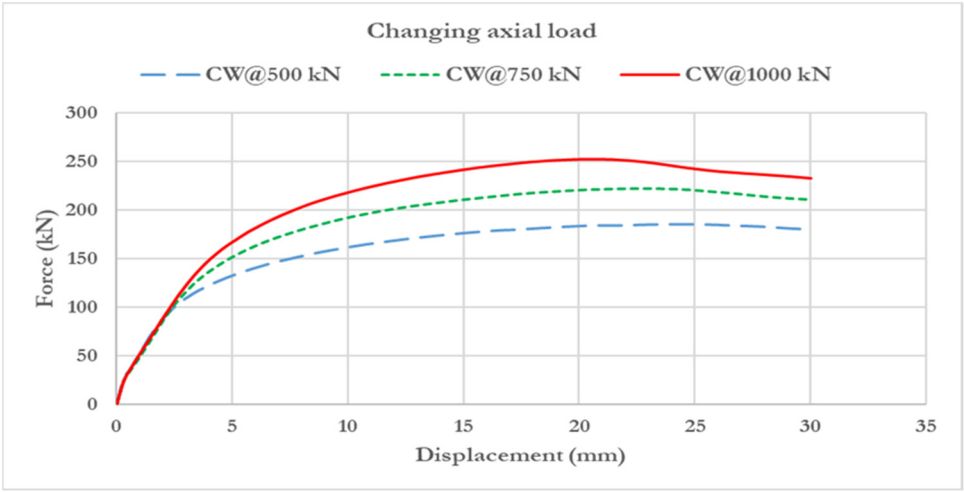

Figure 17. Load–displacement curve for different axial loads on the CW specimen.

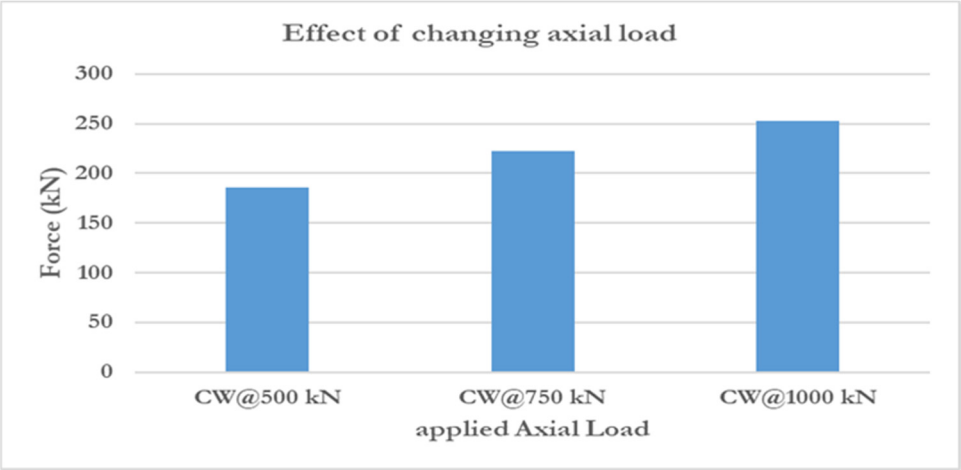

Figure 18. Effect of different axial load ultimate load-carrying capacities.

4.6. Impact of the Compressive Strength of Concrete

The compressive strength of concrete is a crucial factor that can significantly affect various properties and behaviors of concrete structures. Hence, in this research, changing concrete compressive strength was investigated to ascertain the extent of the effect of this factor on the wall specimen strength. For this parameter, four specimens were studied to determine the impact of the compressive strength of concrete. The wall specimens CW-AR2, SW1-AR2, SW4-AR2, and SW7-AR2 are the four specimens that have been studied on this parameter, and their dimensions have been mentioned in Table 4. The initial modulus, the stress–strain relationship, and the concrete-damaged plasticity model are the three criteria that have been followed in ABAQUS [10] to specify concrete material characteristics in the FE simulation. To investigate how compressive strength impacts the behavior of shear walls, the FE models were evaluated using three different values of f'_c, which are 30, 50, and 70 MPa under a constant axial load of 750 kN. Moreover, the four specimens were simulated and subjected to the same loading history to compare the performance of RC shear walls with compressive strengths of 30 MPa and 70 MPa to those with a compressive strength of 50 MPa. Figure 19 shows the specimens used to analyze the impact of compression force on concrete. Based on the numerical analysis outcomes, the results were compared between the four samples of the same wall with an aspect ratio of 2, as demonstrated in Figure 20. It has been observed that the rate of improvement in the bearing capacity of the wall exhibits a decrease as the concrete strength increases while keeping the applied vertical load constant. Specifically, the enhancement rate in wall capacity was determined to be 15.5% when transitioning from a concrete strength of 30 to 50 MPa, and 5.75% when transitioning from 50 to 70 MPa. This underscores the diminishing trend in enhancement as the concrete strength escalates. This can be attributed to the steel rebars' role in controlling the failure mode when a higher concrete strength is used.

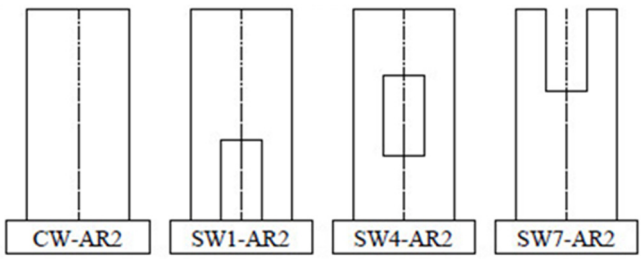

Figure 19. Wall specimens to study concrete compressive strength effect.

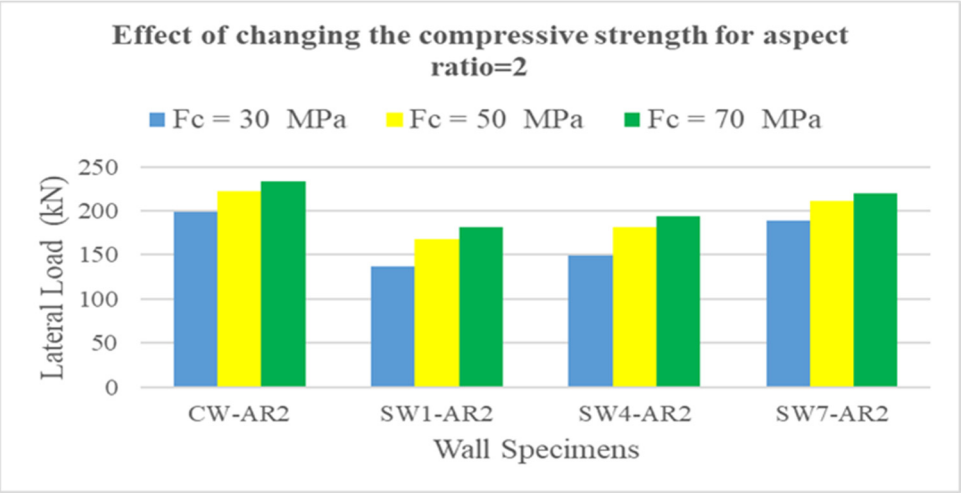

Figure 20. Effect of the compressive strength of concrete for an aspect ratio of 2.0.

5. Discussion

5.1. Stiffness Degradation

In a definition, stiffness is the rigidity of an item. It defines the deformation resistance produced by applied loads. The stiffer an object is considered to be, the greater its resistance to deformation. In buildings, this law applies to determine the stiffness value using the equation below [3].

$$K = \frac{P_{cr}}{\Delta_{cr}} \tag{10}$$

where P_{cr} and Δ_{cr} are the lateral force and displacement at peak load in the elastic region in the curve (linear region), respectively, where the stiffness K represents the ratio of the alteration in load capacity to the corresponding change in displacement. The present study illustrates the calculated stiffness of RC shear walls with different opening areas in Table 9, which demonstrates that augmenting the cross-sectional area results in a proportional decrease in the ultimate secant stiffness, approximately corresponding to the ratio of the opening size.

Table 9. The secant stiffnesses for the SW specimens.

Specimen No	Specimen Label	P_{cr} [kN]	Δ_{cr} [mm]	Stiffness K [kN/mm]	Percentage Decrease
1	CW-R0%	42.200	0.299	141.08	0
2	SW1-R2%	41.619	0.299	139.05	1.44
3	SW1-R5%	40.547	0.299	135.42	4.01
4	SW1-R10%	37.965	0.299	126.78	10.13
5	SW1-R16%	35.464	0.300	118.39	16.08
6	SW1-R21%	32.744	0.300	109.30	22.52
7	SW1-R24%	32.361	0.301	107.69	23.67
8	SW1-R32%	30.046	0.300	100.09	29.05
9	SW1-R42%	28.224	0.301	93.76	33.54

5.2. Ductility

An RC member's ductility is determined by their capacity to withstand significant deformation before failing while keeping a sufficient load capacity in which the ductility value can be used as a direct reflection for estimating the shear wall samples' plastic deformation capability [26]. Hence, determining the ductility number can provide a direct reflection of the capacity. It is typical to utilize two techniques to assess ductility. The first one is the proportion of ultimate deflection to yield deflection. The second one is the deflection at 70 or 80 percent of the maximum loads to guarantee the stiffness reduction

caused by cracking close to the final part of the elastic phase [27]. To determine the ductility factor in the current study, the first approach was applied. According to Equation (11), the ductility index can be defined as the quotient of the ultimate displacement and the yielding displacement.

$$\mu = \frac{\Delta_u}{\Delta_y} \tag{11}$$

Table 10 illustrates the ratios of displacement ductility exhibited by the specimens with various cross-section areas. According to these findings, the wall specimens SW1-R2% and SW1-R10% could show minimal improvements in the ductility index, while the wall specimens SW1-R5%, SW1-R16%, and SW1-R24% showed moderate improvements in the ductility index. Lastly, the ductilities of SW1-R21%, SW1-R32%, and SW1-R42% showed notable improvements, as shown in Table 10.

Table 10. The ductilities of the wall specimens.

Specimen No	Specimen Label	** Δ_y [mm]	* Δ_u [mm]	*** DI	% Increase in the Ductility Index
1	CW-R0%	0.72	13.40	18.61	-
2	SW1-R2%	0.6	14.55	24.25	30.3
3	SW1-R5%	0.4	10.46	26.16	40.5
4	SW1-R10%	0.39	8.32	21.32	14.6
5	SW1-R16%	0.35	10.21	29.18	56.8
6	SW1-R21%	0.30	11.61	38.85	108.7
7	SW1-R24%	0.30	9.19	30.65	64.7
8	SW1-R32%	0.30	12.13	40.43	117.2
9	SW1-R42%	0.30	11.46	38.21	105.3

* Δ_u represents the ultimate deflection, ** Δ_y represents the yield deflection, and *** DI refers to the ductility index.

5.3. Energy Dissipation Capacity

The energy dissipation capacity (E_b) of a member, a property that has long been acknowledged to be of vital importance regarding the structural loading of a structure, can be assessed in several ways. Long et al. [28] have presented a method to calculate the area under the load–displacement curves up to the maximum loads to determine the energy absorption capacity. Table 11 illustrates the calculated values of the ultimate dissipated energy absorption capacity for the wall samples at the aspect ratio of 1.5 and the percentages of energy absorption decrease in the wall specimens. Table 11 shows that the energy absorption capacity decreased with increasing the opening cross-section area.

Table 11. The energy dissipation capacities of the wall specimens.

Specimen No	Specimen Label	Energy Absorption Capacity E_b [kN mm]	Percentage Decrease
1	CW-R0%	4011.94	-
2	SW1-R2%	3936.88	1.87
3	SW1-R5%	3804.75	5.16
4	SW1-R10%	3162.13	21.18
5	SW1-R16%	3156.95	21.31
6	SW1-R21%	2943.25	26.64
7	SW1-R24%	2364.08	41.07
8	SW1-R32%	1803.11	55.06
9	SW1-R42%	321.28	92.00

6. Conclusions

In this study, FE models utilizing nonlinear analysis were established to examine the structural response of RC shear walls featuring cut-out openings. Three groups of shear walls were investigated and differentiated by the effect of their changing size and location

of openings, aspect ratio, axial load, and concrete compressive strength on their structural performance, as shown in Tables 4 and 6. These specimens were designed to withstand a constant axial force. In addition, a static horizontal load was applied to the top of each sample using a displacement control protocol. The main conclusions from this research are drawn as follows:

1. The opening's location greatly affects lateral bearing capacity, energy absorption, and stiffness. The ideal opening placement is at the wall's bottom when the opening is away from the wall center axis, where the wall's load-bearing capacity is lowered by 18%. When the hole is cut into the wall's top, its centralization percentage is 16%.
2. Load-bearing capability depended on the eccentric ratio. The lateral loading capacity drop increased by 8% when the bottom wall opening was created with an eccentric ratio of 0% to 16%. Create the top wall opening with an eccentric ratio from 0% to 16% to reduce lateral loading capacity by 5%.
3. The size ratio lowered wall capacity and stiffness and increased flexibility and displacement. In addition, opening size ratios below 21% demonstrated that opening height had a modest and undetectable effect on concrete wall loading capacity.
4. The opening width exerted a significant influence on the load capacity of the wall. Therefore, it is suggested that any opening in the concrete wall be reduced, the width should not exceed 40% of the total width, and the area of the cut-out hole should not exceed 21% of the entire area of the wall.
5. By increasing the wall aspect ratio, the lateral bearing capacity and stiffness decreased. The aspect ratio of 1.5 was the optimum ratio.
6. This study confirmed that increasing the applied axial load can enhance the lateral bearing capacity of the wall but adversely affect its ductility.
7. This investigation shows that load-bearing capacity decreases with increasing concrete strength under constant vertical load. With an enhancement rate of 15.5% from 30 MPa to 50 MPa and 5.75% from 50 MPa to 70 MPa, the concrete strength of 50 MPa appears to be the most efficient concrete strength for this kind of wall.
8. The stiffness and energy dissipation capacity of the walls decreased with increasing the opening cross-section area, unlike ductility, which increases with the increase in the cross-sectional area of the wall.

Author Contributions: Conceptualization, H.A.M. and M.E.; data curation, M.E. and A.E.-Z.; formal analysis, I.M.S., H.A.M. and S.E.-B.; investigation, I.M.S. and S.E.-B.; methodology, I.M.S., H.A.M. and M.E.; resources, A.E.-Z.; software, A.E.-Z. and S.E.-B.; supervision, H.A.M. and M.E.; validation, I.M.S. and S.E.-B.; visualization, A.E.-Z.; writing—original draft, M.E. and S.E.-B.; writing—review and editing, A.E.-Z. All authors have read and agreed to the published version of the manuscript.

Funding: This research received no external funding.

Data Availability Statement: The data presented in this study are available upon request from the corresponding author.

Conflicts of Interest: The authors declare no conflicts of interest.

References

1. Aslani, K.; Kohnehpooshi, O. Structural behavior of FRP-strengthened reinforced concrete shear walls with openings using finite element method. *Adv. Struct. Eng.* **2018**, *21*, 1072–1087. [CrossRef]
2. Mosallam, A.S.; Nasr, A. Structural performance of RC shear walls with post-construction openings strengthened with FRP composite laminates. *Compos. Part B Eng.* **2017**, *115*, 488–504. [CrossRef]
3. Hosseini, S.A.; Kheyroddin, A.; Mastali, M. An experimental investigation into the impacts of eccentric openings on the in-plane behavior of squat RC shear walls. *Eng. Struct.* **2019**, *197*, 109410. [CrossRef]
4. Yu, H.J.; Kang, S.M.; Park, H.G.; Chung, L. Cyclic loading test of structural walls with small openings. *Int. J. Concr. Struct. Mater.* **2019**, *13*, 40. [CrossRef]
5. ACI. *ACI 318R-19*; Building Code Requirements for Structural Concrete and Commentary. American Concrete Institute (ACI): Farmington Hills, MI, USA, 2019.

6. Liu, M.; Yuan, G.; Sun, W.; Shu, Q.; Zhao, Z.; Lu, L. Experimental and numerical investigation on the seismic performance of RC squat shear walls with single post-opening reinforced by steel plates. *Eur. J. Environ. Civ. Eng.* **2024**, *28*, 53–79. [CrossRef]
7. Mosoarca, M. Failure analysis of RC shear walls with staggered openings under seismic loads. *Eng. Fail. Anal.* **2014**, *41*, 48–64. [CrossRef]
8. Popescu, C.; Sas, G.; Sabău, C.; Blanksvärd, T. Effect of cut-out openings on the axial strength of concrete walls. *J. Struct. Eng.* **2016**, *142*, 04016100. [CrossRef]
9. Li, B.; Qian, K.; Wu, H. Flange effects on seismic performance of reinforced concrete squat walls with irregular or regular openings. *Eng. Struct.* **2016**, *110*, 127–144. [CrossRef]
10. Simulia. *ABAQUS/Standard user's Manual, Volume II Version 6.10*; Hibbitt Karlsson and Sorenson Inc.: Providence, RI, USA, 2010.
11. Ou, Y.C.; Hoang, L.; Roh, H. Cyclic behavior of squat reinforced concrete walls with openings typical of exterior walls of row houses in Taiwan. *Eng. Struct.* **2019**, *195*, 231–242. [CrossRef]
12. Sabau, C.; Popescu, C.; Bagge, N.; Sas, G.; Blanksvärd, T.; Täljsten, B. Local and global behavior of walls with cut-out openings in multi-story reinforced concrete buildings. *Eng. Struct.* **2019**, *187*, 57–72. [CrossRef]
13. Todea, V.; Dan, D.; Florut, S.C.; Stoian, V. Experimental investigations on the seismic behavior of composite steel concrete coupled shear walls with central openings. *Structures* **2021**, *33*, 878–896. [CrossRef]
14. Raza, A.; Khan QU, Z.; Ahmad, A. Numerical Investigation of Load-Carrying Capacity of GFRP-Reinforced Rectangular Concrete Members Using CDP Model in ABAQUS. *Adv. Civ. Eng.* **2019**, *2019*, 1745341. [CrossRef]
15. Husain, M.; Eisa, A.S.; Hegazy, M.M. Strengthening of reinforced concrete shear walls with openings using carbon fiber-reinforced polymers. *Int. J. Adv. Struct. Eng.* **2019**, *11*, 129–150. [CrossRef]
16. Kabaila, A.; Saenz, L.P.; Tulin, L.G.; Gerstle, K.H. Equation for the stress-strain curve of concrete. *ACI J.* **1964**, *61*, 1227–1239. [CrossRef]
17. Hu, H.T.; Schnobrich, W.C. Constitutive modeling of concrete by using nonassociated plasticity. *J. Mater. Civ. Eng.* **1989**, *1*, 199–216. [CrossRef]
18. Kmiecik, P.; Kamiński, M. Modelling of reinforced concrete structures and composite structures with concrete strength degradation taken into consideration. *Arch. Civ. Mech. Eng.* **2011**, *11*, 623–636. [CrossRef]
19. Nielsen, M.P.; Hoang, L.C. *Limit Analysis and Concrete Plasticity*; CRC Press: Boca Raton, FL, USA, 2016. [CrossRef]
20. Nayal, R.; Rasheed, H.A. Tension stiffening model for concrete beams reinforced with steel and FRP bars. *J. Mater. Civ. Eng.* **2016**, *18*, 831–841. [CrossRef]
21. Lubliner, J.; Oliver, J.; Oller, S.; Oñate, E. A plastic-damage model for concrete. *Int. J. Solids Struct.* **1989**, *25*, 299–326. [CrossRef]
22. Birtel, V.; Mark, P. Parameterised finite element modelling of RC beam shear failure. In Proceedings of the ABAQUS Users' Conference, Cambridge, MA, USA, 23–25 May 2006; Volume 14, pp. 95–108.
23. Canadian Standards Association. *A23.3-04*; Design of Concrete Structures. Canadian Standards Association: Mississauga, ON, Canada, 2004.
24. Wang, J.Y.; Sakashita, M.; Kono, S.; Tanaka, H.; Lou, W.J. Behavior of reinforced concrete structural walls with various opening locations: Experiments and macro model. *J. Zhejiang Univ. Sci. A* **2010**, *11*, 202–211. [CrossRef]
25. Wang, J.; Sakashita, M.; Kono, S.; Tanaka, H. Shear behaviour of reinforced concrete structural walls with eccentric openings under cyclic loading: Experimental study. *Struct. Des. Tall Spec. Build.* **2012**, *21*, 669–681. [CrossRef]
26. Emara, M.; Rizk, M.; Mohamed, H.; Zaghlal, M. Enhancement of circular RC columns using steel mesh as internal or external confinement under the influence of axial compression loading. *Frat. Integrità Strutt.* **2021**, *15*, 86–104. [CrossRef]
27. Salonikios, T.N.; Kappos, A.J.; Tegos, I.A.; Penelis, G.G. Cyclic load behavior of low-slenderness reinforced concrete walls: Failure modes, strength and deformation analysis, and design implications. *ACI Struct. J.* **2000**, *97*, 132–141.
28. Long, N.-M.; Phuong, P.-V.; Duong, T.-T.; Quynh, P.T.T.; Thong, M.P.; Cuong, N.-H.; Rovňák, M. Flexural-strengthening efficiency of CFRP sheets for unbonded post-tensioned concrete T-beams. *Eng. Struct.* **2018**, *166*, 1–15. [CrossRef]